Supporting Information for

Phase separation at the nanoscale quantified by dcFCCS

Sijia Peng [1#], Weiping Li [1#], Yirong Yao [1#], Wenjing Xing [1], Pilong Li [*1], Chunlai Chen [*1]

1 School of Life Sciences; Tsinghua-Peking Joint Center for Life Sciences; Beijing Advanced Innovation Center for Structural Biology; Beijing Frontier Research Center for Biological Structure, Tsinghua University, Beijing, 100084, China.

# these authors contributed equally to this work

* To whom correspondence should be addressed. Email: chunlai@mail.tsinghua.edu.cn (CC) & pilongli@mail.tsinghua.edu.cn (PL)

This PDF file includes:

www.pnas.org/cgi/doi/10.1073/pnas.2008447117

Methods and Materials

Common materials

Alexa Fluor® 488 (1 mg, maleimide) was purchased from Invitrogen. Sulfo Cyanine5 (1 mg, maleimide), Sulfo Cyanine5 (1 mg, NHS ester), and Sulfo Cyanine3 (1 mg, NHS ester) were purchased from Lumiprobe. UltraPure™ 1M Tris-HCI pH 7.5 and nuclease-free water were obtained from Invitrogen. Other common materials and reagents were purchased from Sigma or Amresco.

Plasmid construction, protein purification and labeling

Plasmids with genes encoding yeast SmF (ySmF) variants were constructed using the pRSF Duet1 (Novagen). A linker sequence encoding GGSGGSGGSGGSGGS**C**GGS connects ySmF and a short peptide KKETPV or PDZ domain or SH3 domain or PRM domain. Single cysteine mutation in the linker region, which was used for labeling, was created by site-directed mutagenesis and confirmed by DNA sequencing. All proteins were expressed in BL21(DE3) T1R cells (Tiangen) at 18 °C through overnight induction with 1 mM isopropyl-beta-D-thiogalactopyranoside (IPTG). Cells were collected by centrifuge and then lysed using Ultrasonic Cell Disruptor (Nanjing Xinchen Biotechnology Company) in 40 mM Tris-HCl pH 7.4, 500 mM NaCl and 1 mM PMSF. Cell lysates were clarified using centrifugation. The supernatants were loaded onto the Ni-NTA agarose (Qiagen, Venlo, Netherlands), washed with the washing buffer (40 mM Tris-HCl pH 7.4, 500 mM NaCl and 40 mM imidazole), and eluted with the elution buffer (40 mM Tris-HCl pH 7.4, 500 mM NaCl and 500 mM imidazole). The proteins were further purified using a Hitrap Q column (GE Healthcare). The MBP-SUMO tag was cleaved by overnight incubation with ULP1 and removed by tandem Ni and MBP column (GE Healthcare). Lastly, the proteins were further purified using an SD200 column (GE Healthcare) with 40 mM Tris-HCl pH 7.4, 150 mM NaCl and 1 mM TCEP.

Maleimide derived fluorophores and cysteine-containing ySmF variants were mixed at 50:1 molar ratio in reaction buffer (50 mM Tris-HCl pH 7.5, 150 mM NaCl and 1 mM TCEP) and incubated at room temperature for two hours. Labeled proteins were separated from excess free fluorophores through a desalting Sephadex G-25 column (Nap-5, GE). For Alexa 488-KKETPV$_{14}$ and Cy5-PDZ$_{14}$, the labeling efficiency of ySmF monomer is 80% ± 1% and 99% ± 4%, respectively.

RNA transcription, purification and labeling

Template double-stranded DNAs (Table S3) were generated via polymerase chain reaction (Q5 high-fidelity PCR kit, NEB) using two single-stranded partially complementary oligonucleotides (Sangon Biotech, Shanghai). dsDNAs with correct length were recovered from agarose gels. RNAs were transcribed using the HiScribe T7 kit (NEB), purified on a 10% denaturing (8 M urea) polyacrylamide gel and resuspended in nuclease-free water.

For RNA labeling, amino-UTP (Thermo Fisher Scientific) was included in transcription reaction mixtures to transcribe amino derived RNA. Sulfo Cyanine5 or Sulfo Cyanine3 (NHS ester) and amino-RNA were mixed at 20:1 molar ratio in 10 mM $NaHCO_3$ buffer and were incubated in the dark at ~23 °C for 4 h. Labeled RNAs were purified via ethanol precipitation for three times. Pellet was dried in the air and dissolved in nuclease-free water.

Phase separation examined by conventional fluorescence microscopy

For phase separation of ySmF variants, experiments were performed with 384 low-binding multi-well microscopy plates (Greiner, 781096). Proteins were mixed into the reaction buffer (50 mM Tris-HCl pH 7.5, 150 mM NaCl and 1 mM TCEP) at room temperature and visualized using a PerkinElmer High Content Screening System Opera Phenix microscope equipped with a 63× water immersion objective. Harmony 4.8 was used to analyze the images.

Cy3 and Cy5 labeled RNAs were diluted in 10 mM Tris-HCl pH 7.0, 10 mM $MgCl_2$, 25 mM NaCl or 50 mM NaCl, unless indicated otherwise. RNAs were denatured at 95 ℃ for 3 min and cooled down at 1 ℃ per min to 37 ℃ in a thermocycler. Samples were visualized using a spinning disk confocal microscope (Olympus IX83) equipped an oil-immersion objective (100×, NA = 1.4) and an air-cooled EMCCD.

Preparation of PEG-passivated slides

PEG-passivated slides were prepared according to previous procedure with minor modifications (1, 2). In brief, slides and coverslips were sonicated at 40 ºC in the order of ethanol (10 minutes), 0.2 M KOH (20 minutes), and ethanol (10 minutes). Cleaned slides and coverslips were treated with amino-silane reagents (1 ml 3-Aminopropyltriethoxysilane, 5 ml acetic acid, and 94 ml methanol) at

room temperature overnight and then incubated with polyethylene glycol (PEG, Laysan Bio, Inc., containing 20% w/w mPEG-Succinimidyl Valerate, MW 2,000) in 0.1 M sodium bicarbonate (pH 8.3) for 3 h. Slides and coverslips were dried by clean N_2, put in 50 mL falcon tubes, vacuum sealed in food saver bags, and stored at -20 ºC.

Fluorescence recovery after photobleaching (FRAP) assay

FRAP assay was performed on a Nikon confocal microscope at room temperature, equipped with a 100× oil immersion objective. The fluorescence intensity of prebleach was normalized to 100%. Liquid droplet images were captured in a low-binding 384 multi-well 0.17 mm microscopy plates (Cellvis, P384-1.5H-N). All data were collected within 90 min after LLPS formation.

Negative-stain electron microscopy

To prepare the negative-staining specimen, 4 μL of the reaction mixture containing Alexa 488-$(KKETPV)_{14}$ and Cy5-PDZ_{14} after 1 hour incubation was absorbed on 300-mesh carbon-coated copper grids (Beijing Zhongjingkeyi Technology) for 1 min. Then, the grids were stained with 2% uranyl acetate solution (wt/vol). Filter paper was used to absorb the redundant uranyl acetate until grids surface was dry. The grids were visualized using an FEI Technai Spirit transmission electron microscope equipped with an FEI eagle 4k charge-coupled device (CCD) camera.

Monte Carlo simulation to mimic formation and growth of heterocomplex and condensate

Three assumptions were made to construct our simulation. 1) Within any particle, the molecular ratio of $KKETPV_{14}$:PDZ_{14} is between 1/3 and 3. This boundary condition is enforced throughout the simulation. 2) Any two molecules or particles can bind to each other to form large particles when satisfying assumption 1. A constant second-order reaction rate k_{on} is used to define binding rate between any two molecules or particles, which is based on two points. Firstly, diffusion-driven collision rate is insensitive to the size of particles (3). Because, the simplest geometry to describe the collision rate (k_{co}) of two spherical particles A and B is $k_{co} = 4\pi(D_A + D_B)(r_A + r_B)$, in which D_A and D_B are diffusion constants, and r_A and r_B are the radii of particles A and B, respectively. According to Strokes-Einstein relation, hydrodynamic radii of molecules are described via $r_H = \frac{k_B T}{6\pi\eta D}$,

in which k_B is the Boltzman's constant, T is the absolute temperature, η is the solution viscosity and D is diffusion coefficient. Assuming the hydrodynamic radii of particles A and B are similar, k_{co} will be given, in approximate, as $k_{co} = 8k_BT/3\eta$, which is insensitive to the size of particles. Secondly, when the size of particles is relative small throughout the simulation, we assume the efficiency for two particles to bind after collision remains mostly the same. 3) Surface-exposed $KKETPV_{14}$ and PDZ_{14} molecules can dissociate from a particle via the following parallel reaction pathways, respectively.

$(KKETPV_{14})_N(PDZ_{14})_M \rightarrow (KKETPV_{14})_{N-1}(PDZ_{14})_M + KKETPV_{14}$

$(KKETPV_{14})_N(PDZ_{14})_M \rightarrow (KKETPV_{14})_N(PDZ_{14})_{M-1} + PDZ_{14}$

N and M are the number of $KKETPV_{14}$ and PDZ_{14} molecules in the particle, respectively. The dissociation rates of these two pathways are $N^{\frac{2}{3}}k_{off}$ and $M^{\frac{2}{3}}k_{off}$, respectively, in which $N^{\frac{2}{3}}$ and $M^{\frac{2}{3}}$ are used to roughly estimate the number of surface exposed $KKETPV_{14}$ and PDZ_{14} molecules, respectively.

Simulation is carried out using Matlab installed on a regular office computer. To focus on formation of nanoscale condensate, the upper limit of $KKETPV_{14}$ molecules in each particle is set to 100 and the upper limit of PDZ_{14} molecules is also 100. Based on 3 assumptions describe above and concentrations of all species at time t, concentrations of all species after a small simulation time step (Δt, set as 0.01 min) are calculated, which are used to estimate concentrations after another simulation time step. Through this iteration approach, we estimated the concentration of different heterocomplexes over time using different initial concentrations of $KKETPV_{14}$ and PDZ_{14}, with which A_x/A_{488} was calculated. Using k_{on} = 0.034 $min^{-1}nM^{-1}$ and k_{off} = 0.22 min^{-1}, our simulated A_x/A_{488} curves were quite similar to measured curves (Figs. 2D and F), which validated our simulation model.

Clustering analysis

To perform a two-dimensional clustering analysis, hydrodynamic volumes of heterocomplexes and increasing of their volumes after 1 hour incubation were calculated from relaxation times of dcFCCS curves under different concentrations of ySmF monomers (Table S1). Lloyd's algorithm (4), an iterative data-partitioning algorithm included in a built-in matlab function, was used to assign all data points into two clusters while minimizing the sum of point-to-centroid distances.

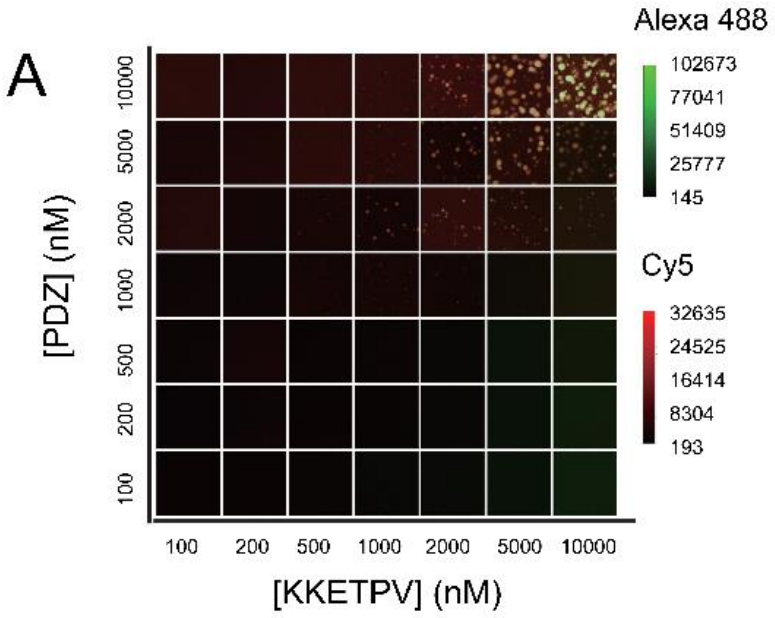
A
Alexa 488
102673
77041
51409
25777
145
Cy5
32635
24525
16414
8304
193
[PDZ] (nM)
10000
5000
2000
1000
500
200
100
100 200 500 1000 2000 5000 10000
[KKETPV] (nM)

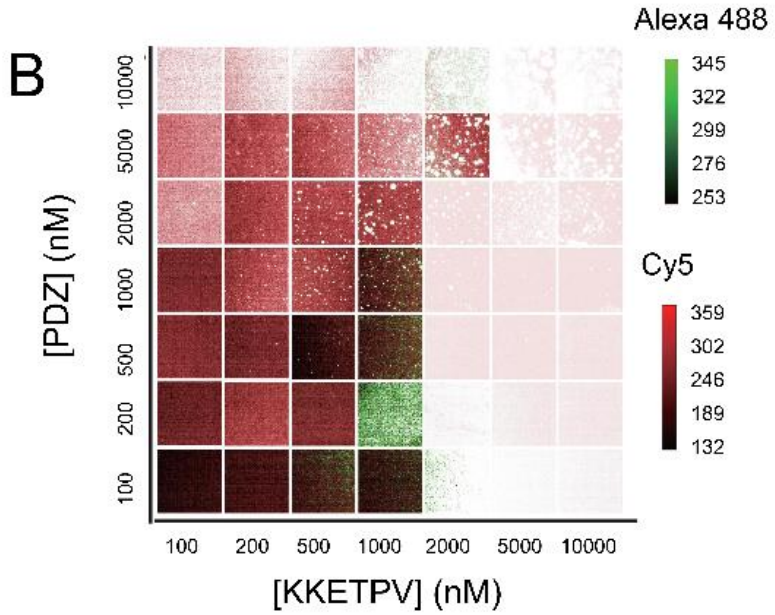
B
Alexa 488
345
322
299
276
253
Cy5
359
302
246
189
132
[PDZ] (nM)
10000
5000
2000
1000
500
200
100
100 200 500 1000 2000 5000 10000
[KKETPV] (nM)

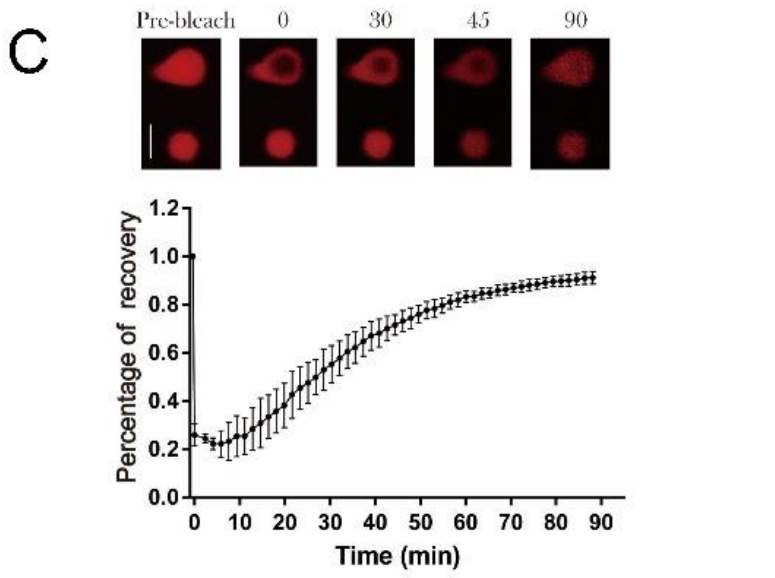
C
Pre-bleach
0
30
45
90
Percentage of recovery
1.2
1.0
0.8
0.6
0.4
0.2
0.0
0 10 20 30 40 50 60 70 80 90
Time (min)

Fig. S1. Liquid droplets formation using mixtures of Alexa 488-KKETPV$_{14}$ and Cy5-PDZ$_{14}$. A-B) Liquid droplets observed using high-content confocal fluorescence microscopy under different concentrations. The same images were plotted using different contrast to clearly show droplets formed at high concentrations **(A)** and at low concentrations **(B)**, respectively. Concentrations of ySmF monomers were listed. **C)** Fluorescence recovery after photobleaching (FRAP) curve of Cy5-PDZ$_{14}$ after internal photobleaching of KKETPV$_{14}$-PDZ$_{14}$ droplets formed at 10 μM of Alexa 488-KKETPV$_{14}$ and Cy5-PDZ$_{14}$. Values shown are the mean ± SD, n = 6. Scale bar, 1 μm.

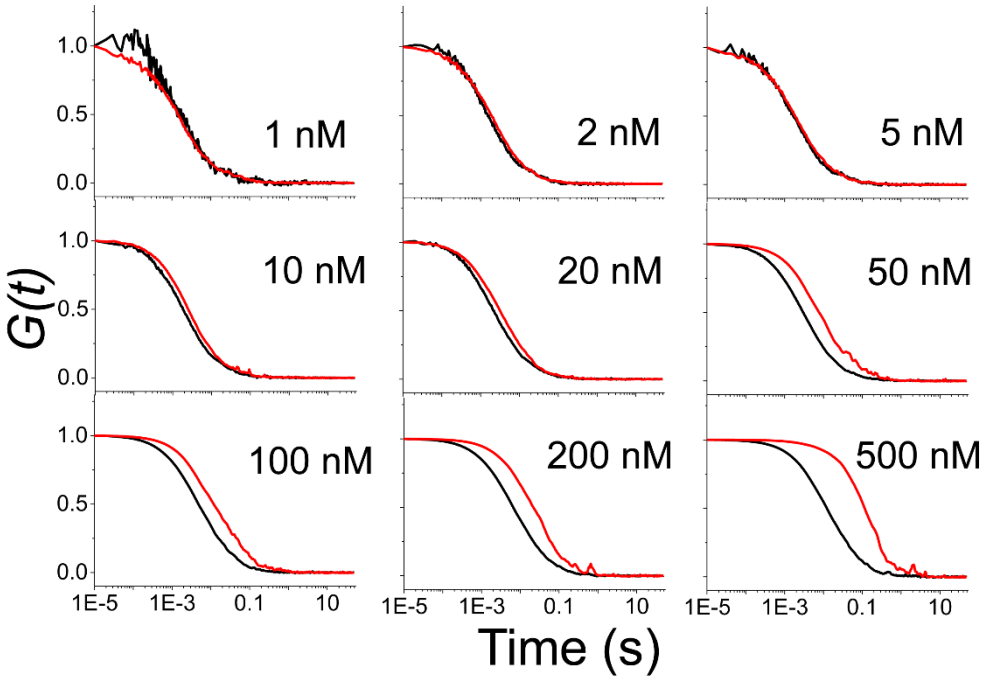

Fig. S2. Normalized dcFCCS curves of mixtures of Alexa 488-KKETPV$_{14}$ and Cy5-PDZ$_{14}$ under different concentrations. dcFCCS curves were taken right after mixing (black curves) and after 1 hour (red curves). Concentrations of ySmF monomers were listed.

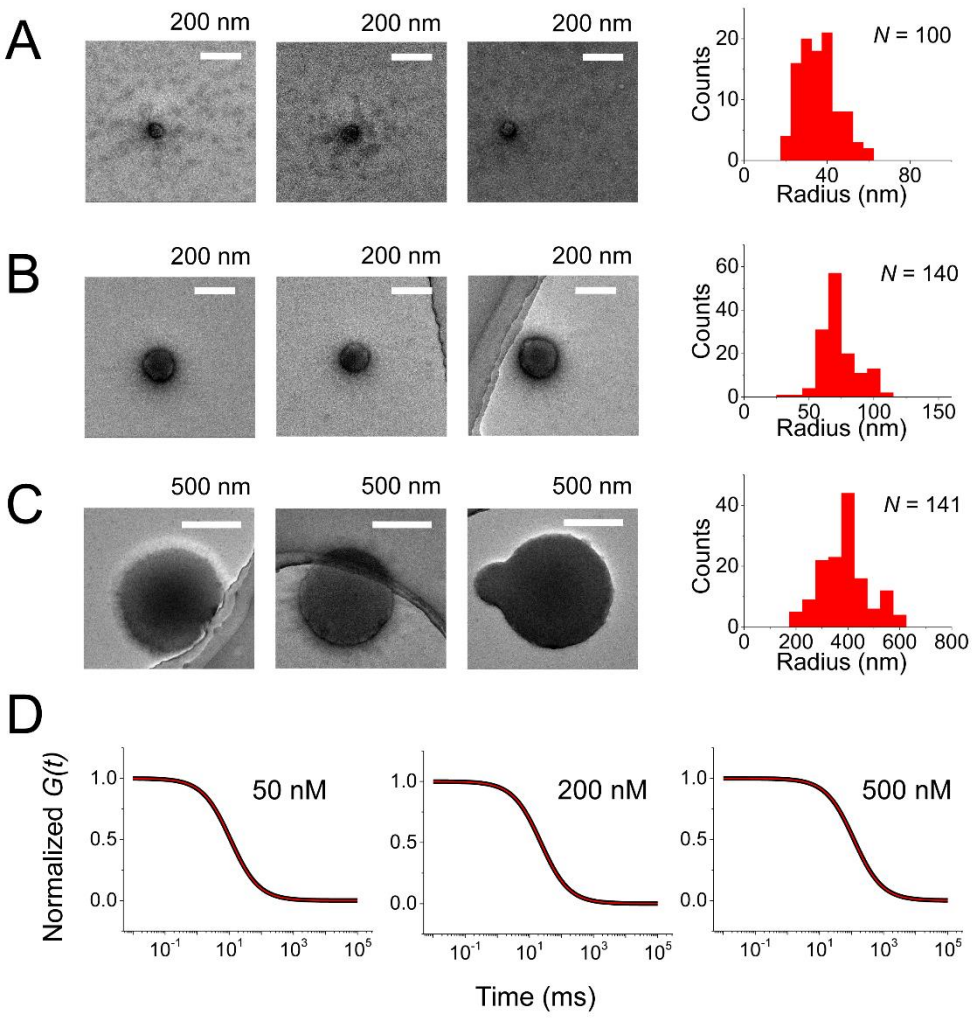

Fig. S3. KKETPV$_{14}$-PDZ$_{14}$ condensates examined by negative-stain transmission electron microscopy. A-C) Equal amount of Alexa 488-KKETPV$_{14}$ and Cy5-PDZ$_{14}$ were mixed at 50 nM **(A)**, 200 nM **(B)** and 500 nM **(C)** and were incubated for 1 hour before negative staining. Scale bars and their size distributions are listed. The average radii of condensates measured by negative-stain transmission electron microscopy were 36 ± 9 nm, 73 ± 14 nm and 390 ± 90 nm, respectively. **(D)** Simulated dcFCCS curves (black curves) of condensates generated from their size distributions shown in **(A-C).** A single-component diffusion model (red curves) is sufficient to fit these simulated dcFCCS curves to estimate their average radii (35 nm, 72 nm, and 380 nm, respectively), which agreed with the data used to generate the simulated curves.

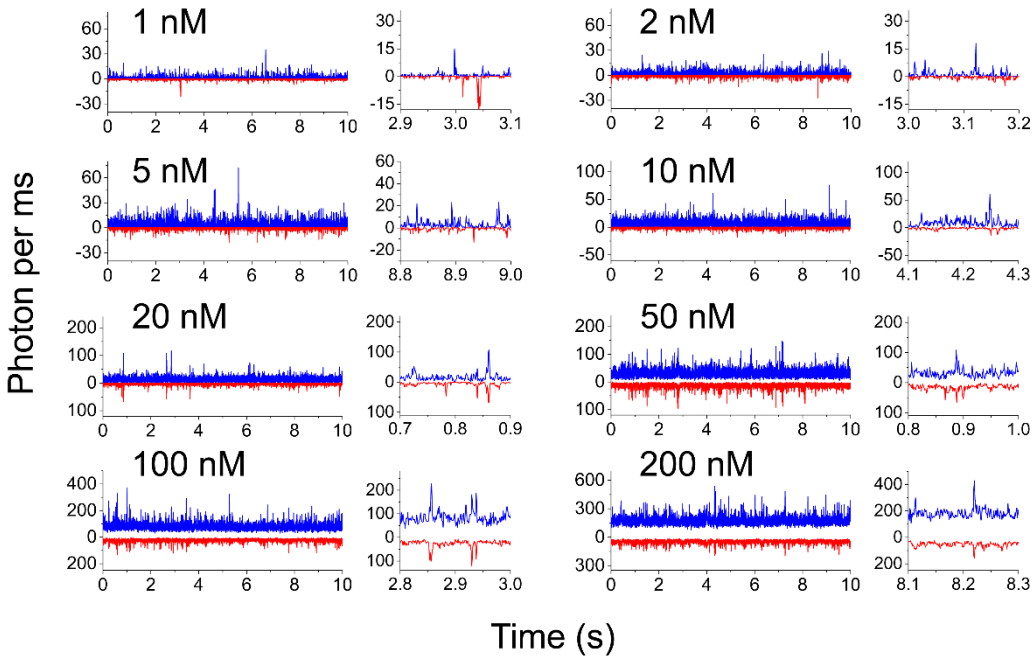

Fig. S4. 1ms-binned fluorescence trajectories of mixtures of Alexa 488-KKETPV$_{14}$ and Cy5-PDZ$_{14}$ under different concentrations. Zoom-in trajectories are shown on the right. Laser powers of 488 nm and 640 nm lasers were ~2.5 μW.

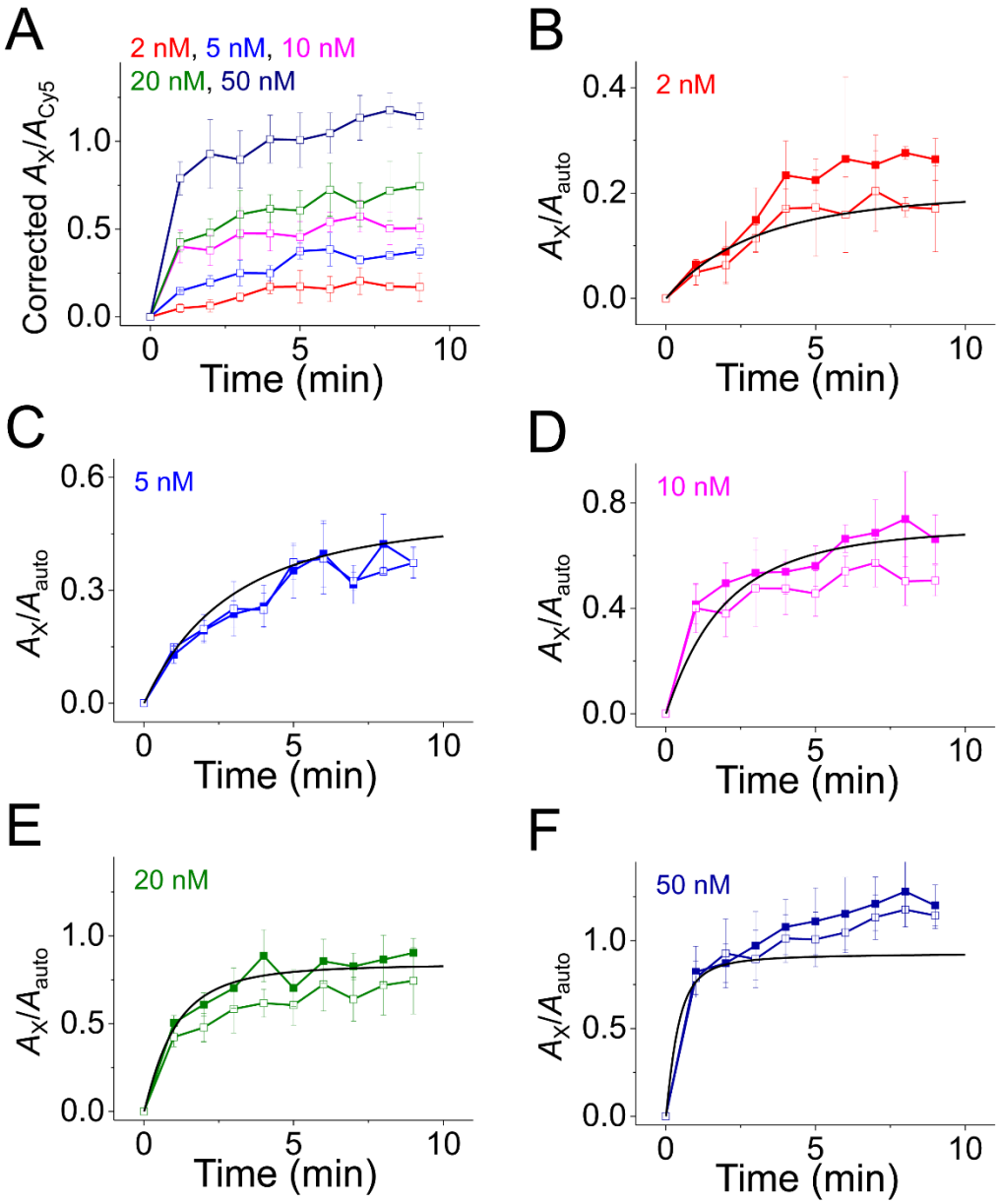

Fig. S5. Change of A_x/A_{auto} in the first 10 min calculated from dcFCCS measurements and estimated by Monte Carlo simulation. A) Increase of measured A_x/A_{Cy5} in the first 9 min after mixing. **B-F)** Measured A_x/A_{488} (Fig. 2D) and A_x/A_{Cy5} and simulated A_x/A_{auto} (Fig. 2F) are plotted together for direct comparison. Measured A_x/A_{488} and A_x/A_{Cy5} are in solid and hollow dots, respectively. Simulated A_x/A_{auto} are plotted in black curves. A_{auto} is the amplitude of auto-correlation curve of Alexa 488 channel and Cy5 channel, whose simulated values are the same when the concentrations of Alexa 488-KKETPV$_{14}$ and Cy5-PDZ$_{14}$ are the same.

.

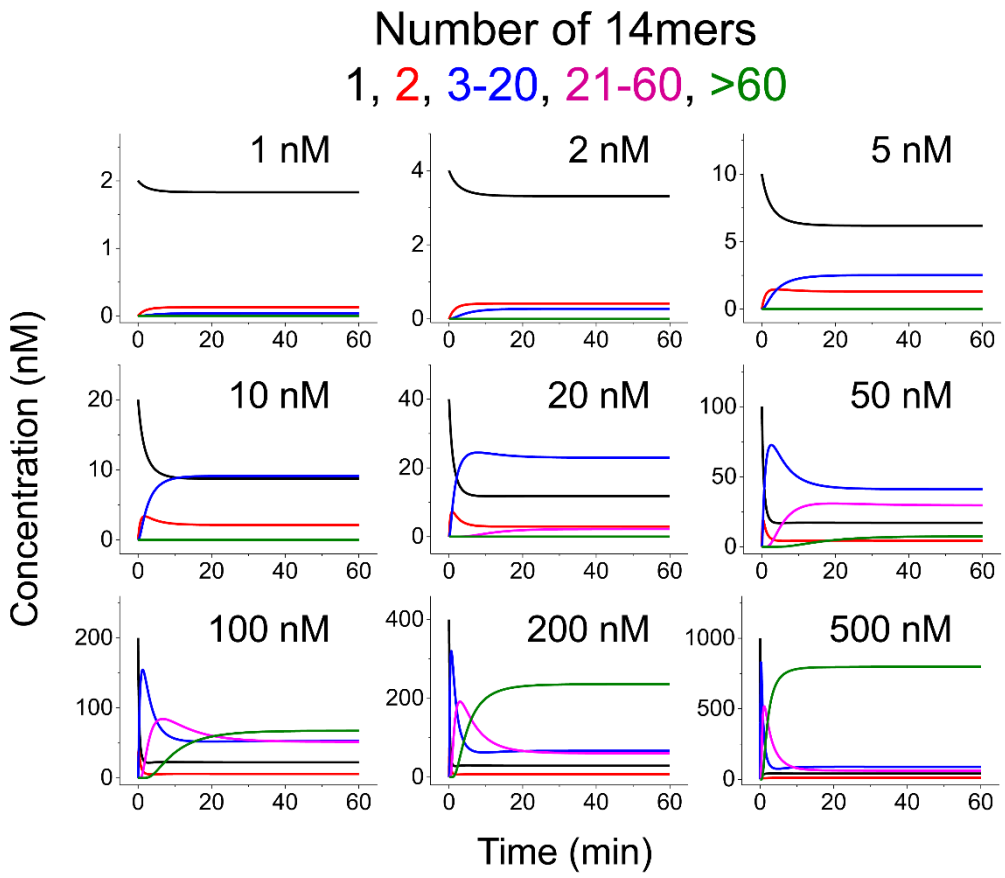

Fig. S6. Concentrations of KKETPV$_{14}$, PDZ$_{14}$, and heterocomplexes of different sizes over time estimated by Monte Carlo simulation under different initial concentrations. For clarity, heterocomplexes were divided into four groups containing 2, 3-20, 21-60 and >60 14-mers, respectively. KKETPV$_{14}$ and PDZ$_{14}$ were combined into one group containing only 1 14-mer. All concentrations were converted to effective concentrations of ySmF monomers. k_{on} = 0.034 min^{-1}nM^{-1} and k_{off} = 0.22 min^{-1} were used in simulation. More details of simulation are described in the methods section.

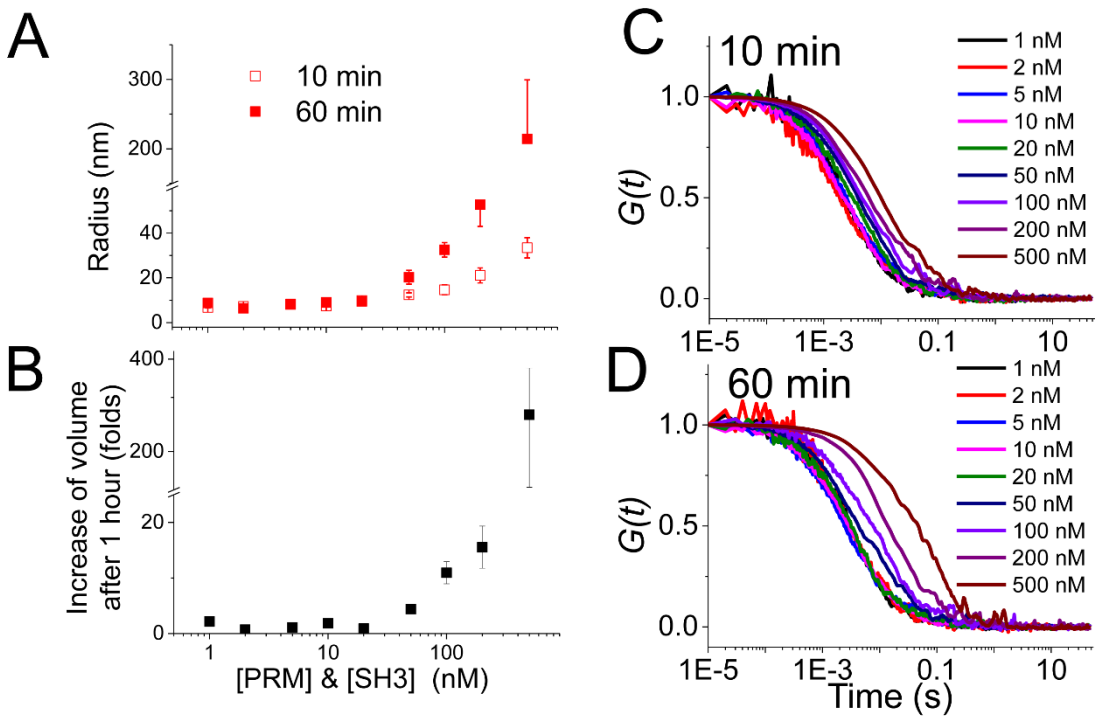

Fig. S7. Quantification of PRM_{14}-$SH3_{14}$ heterocomplexes and condensates formation. A) Hydrodynamic radius of PRM_{14}-$SH3_{14}$ heterocomplexes extracted from relaxation times of dcFCCS curves. **B)** Increasing of hydrodynamic volume after 1 hour incubation. **C and D)** Normalized dcFCCS curves of mixtures of Alexa 488-PRM_{14} and Cy5-$SH3_{14}$ under different concentrations. dcFCCS curves were taken right after mixing (C) and after 1 hour (D). Concentrations of ySmF monomers were listed.

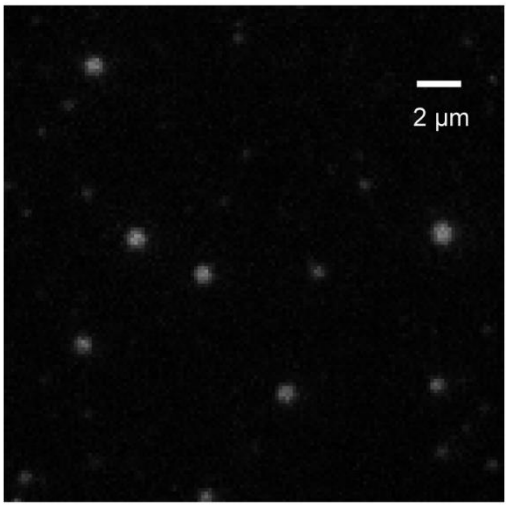

Fig. S8. Fluorescence imaging of Alexa 488-PDZ recruited by phase-separated PRM_{14}-$(SH3\text{-}KKETPV)_{14}$ condensates. Fluorescence signals of Alexa 488 were collected by a total internal reflection fluorescence (TIRF) microscope. 4 μM PRM_{14} and 2 μM $(SH3\text{-}KKETPV)_{14}$ were used to form condensates to recruit 200 nM Alexa 488-PDZ. Average intensity of condensates, whose diameters were larger than 1 μm, was 1160 ± 220 (a.u.). Background intensity caused by free Alexa 488-PDZ in aqueous solution was 34 ± 5 (a.u.). Together, PDZ is enhanced by 34 ± 6 fold within condensates.

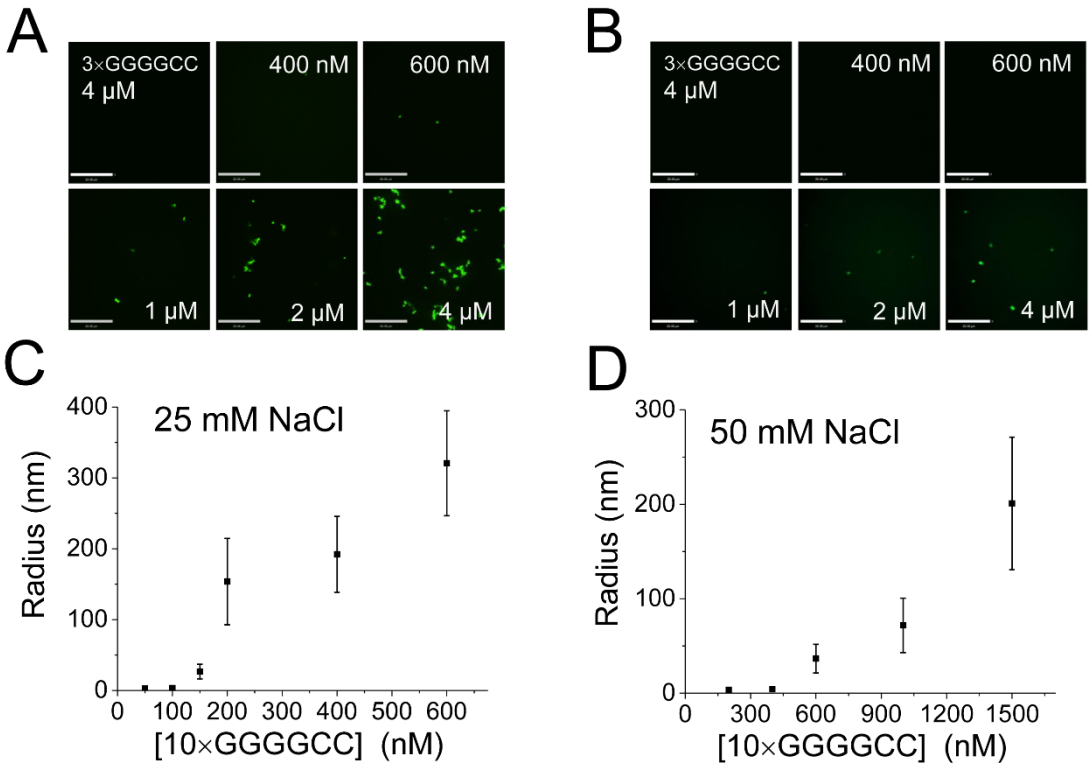

Fig. S9. RNA Condensates formation examined using confocal fluorescence microscopy and dcFCCS assay. A and B) Condensates formed from RNAs containing 10×GGGGCC sequence captured by spinning disk confocal fluorescence microscopy under different concentrations with buffers containing 25 mM NaCl (A) or 50 mM NaCl (B). Scale bar is 20 μm. RNA containing 3×GGGGCC was used as the negative control. **C and D)** Hydrodynamic radius of RNA condensates calculated from relaxation times of dcFCCS curves under different concentrations with buffers containing 25 mM NaCl (C) or 50 mM NaCl (D).

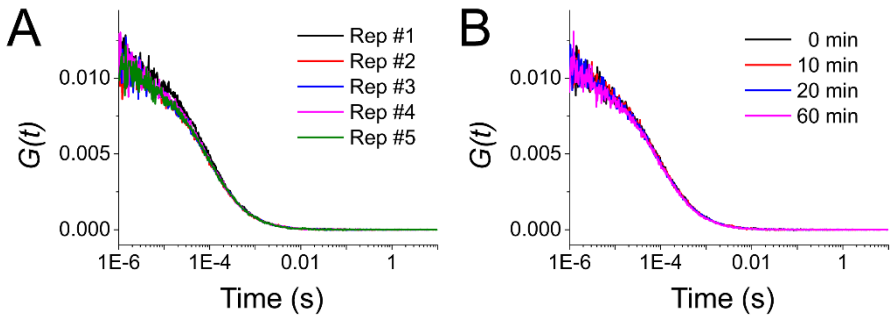

Fig. S10. Auto-correlation curves of Alexa 488. A) Five identical replicates, whose relaxation times were 86 ± 1 μs, 90 ± 2 μs, 90 ± 2 μs, 86 ± 1 μs and 91 ± 2 μs. **B)** Auto-correlation curves taken 0, 10, 20 and 60 min after adjusting focus, whose relaxation times were 91 ± 2 μs, 91 ± 2 μs, 88 ± 1 μs and 87 ± 1 μs, respectively. All curves were calculated from 1-min-length fluorescence trajectories.

.

Table S1. Relaxation times (ms) of mixtures of Alexa 488-$KKETPV_{14}$ and Cy5-PDZ_{14} under different concentrations of ySmF monomers measured right after mixing (black) and after 1 hour incubation (red).

[PDZ]	[KKETPV]								
	1 nM	2 nM	5 nM	10 nM	20 nM	50 nM	100 nM	200 nM	500 nM
1 nM	1.5 ± 0.2	1.7 ± 0.3	1.8 ± 0.1	1.6 ± 0.3	1.9 ± 0.2	1.9 ± 0.3	1.4 ± 0.4	1.9 ± 0.2	2.2 ± 0.4
	1.6 ± 0.1	1.9 ± 0.1	1.8 ± 0.1	2.0 ± 0.3	1.7 ± 0.2	2.3 ± 0.2	1.7 ± 0.7	2.5 ± 0.7	2.4 ± 0.2
2 nM	1.4 ± 0.1	1.5 ± 0.1	1.7 ± 0.1	1.7 ± 0.1	1.8 ± 0.1	1.6 ± 0.1	2.3 ± 0.3	2.0 ± 0.4	1.7 ± 0.3
	1.9 ± 0.1	2.0 ± 0.1	2.2 ± 0.2	1.9 ± 0.1	2.2 ± 0.2	2.3 ± 0.2	2.3 ± 0.2	2.5 ± 0.4	2.6 ± 0.2
5 nM	1.5 ± 0.3	1.7 ± 0.4	1.7 ± 0.1	1.8 ± 0.1	1.7 ± 0.2	2.0 ± 0.2	1.9 ± 0.2	1.9 ± 0.2	2.0 ± 0.3
	2.3 ± 0.1	2.5 ± 0.1	2.2 ± 0.1	2.5 ± 0.2	2.2 ± 0.1	2.4 ± 0.1	2.1 ± 0.1	2.7 ± 0.4	2.7 ± 0.5
10 nM	1.6 ± 0.1	1.8 ± 0.1	1.6 ± 0.1	1.8 ± 0.1	2.1 ± 0.2	1.9 ± 0.2	2.2 ± 0.4	2.0 ± 0.1	2.2 ± 0.1
	1.9 ± 0.1	2.1 ± 0.2	2.6 ± 0.1	2.7 ± 0.3	2.5 ± 0.3	2.1 ± 0.2	2.8 ± 0.6	2.2 ± 0.1	2.2 ± 0.2
20 nM	1.6 ± 0.1	1.8 ± 0.1	1.7 ± 0.1	2.4 ± 0.2	2.2 ± 0.2	2.3 ± 0.2	2.5 ± 0.3	2.4 ± 0.1	2.7 ± 0.3
	2.0 ± 0.4	1.8 ± 0.2	2.5 ± 0.1	4.0 ± 0.2	3.8 ± 0.4	4.3 ± 0.1	3.4 ± 0.5	3.4 ± 0.8	3.6 ± 0.5
50 nM	1.9 ± 0.3	1.8 ± 0.2	2.0 ± 0.1	1.9 ± 0.1	2.6 ± 0.3	3.0 ± 0.1	3.2 ± 0.4	2.9 ± 0.2	3.5 ± 0.4
	2.5 ± 0.4	1.8 ± 0.1	2.6 ± 0.4	2.5 ± 0.3	5.6 ± 0.2	7.3 ± 0.5	11 ± 2	9 ± 3	8 ± 1
100 nM	1.4 ± 0.1	1.5 ± 0.1	1.7 ± 0.1	1.7 ± 0.1	2.3 ± 0.2	4.4 ± 0.3	4.6 ± 0.3	5.0 ± 0.9	4.5 ± 0.2
	1.3 ± 0.1	1.5 ± 0.1	3 ± 1	3.2 ± 0.1	3.9 ± 0.3	12 ± 1	13 ± 1	18 ± 5	10 ± 2
200 nM	1.5 ± 0.2	1.6 ± 0.2	1.5 ± 0.1	1.9 ± 0.1	2.0 ± 0.1	3.3 ± 0.3	4.6 ± 0.5	5.7 ± 0.4	7 ± 1
	1.3 ± 0.2	1.4 ± 0.1	1.8 ± 0.1	2.3 ± 0.1	3.7 ± 0.2	9.6 ± 0.8	19 ± 4	19 ± 2	30 ± 4
500 nM	2.1 ± 0.5	1.5 ± 0.2	1.9 ± 0.4	1.7 ± 0.1	1.9 ± 0.3	2.9 ± 0.3	4.3 ± 0.3	10 ± 2	10.9 ± 0.7
	2.0 ± 0.4	2.1 ± 0.5	2.6 ± 0.6	1.9 ± 0.2	3.1 ± 0.3	9 ± 1	16 ± 2	60 ± 30	110 ± 20

Table S2. Growth rate of condensate radius ($nm \cdot min^{-1}$) in the first 9 min after mixing under different concentrations of ySmF monomers.

[PDZ]	[KKETPV]				
	20 nM	50 nM	100 nM	200 nM	500 nM
20 nM	0.2 ± 0.1	0.2 ± 0.2	0.3 ± 0.1	0.1 ± 0.1	0.3 ± 0.3
50 nM	0.1 ± 0.1	0.5 ± 0.1	1.0 ± 0.3	0.5 ± 0.3	0.5 ± 0.5
100 nM	0.2 ± 0.2	1.1 ± 0.2	0.9 ± 0.2	1.1 ± 0.3	0.6 ± 0.3
200 nM	0.1 ± 0.2	0.4 ± 0.1	1.0 ± 0.1	1.5 ± 0.2	4.0 ± 1.0
500 nM	0.4 ± 0.3	0.3 ± 0.3	0.8 ± 0.4	2.8 ± 0.9	4.7 ± 0.3

Table S3. Template sequences for RNA transcription

Name	Sequences (from 5’ to 3’)
3×GGGGCC	TAATACGACTCACTATAGGGAGAGGGGCCGGGGCCGGG GCCTCTCCCTTTAGTGAGGGTTAATTGAGCTCA
10×GGGGCC	TAATACGACTCACTATAGGGAGAGGGGCCGGGGCCGGG GCCGGGGCCGGGGCCGGGGCCGGGGCCGGGGCCGGGG CCGGGGCCTCTCCCTTTAGTGAGGGTTAATTGAGCTCA

Sequence of one strand of dsDNA was listed.

SI References

1. Ha T, *et al.* (2002) Initiation and re-initiation of DNA unwinding by the Escherichia coli Rep helicase. *Nature* 419(6907):638-641.
2. Peng S, Sun R, Wang W, & Chen C (2017) Single-Molecule Photoactivation FRET: A General and Easy-To-Implement Approach To Break the Concentration Barrier. *Angewandte Chemie* 56(24):6882-6885.
3. Berg OG & Vonhippel PH (1985) Diffusion-Controlled Macromolecular Interactions. *Annu Rev Biophys Bio* 14:131-160.
4. Lloyd SP (1982) Least-Squares Quantization in Pcm. *Ieee T Inform Theory* 28(2):129-137.